applied sciences

MDPI

Article

Integration of Sensors for Enhanced Condition Monitoring in Polymer Gears: A Comparative Study of Acceleration and Temperature Sensors

Sascha Hasenoehrl, Julian Peters and Sven Matthiesen *

Institute of Product Engineering, Karlsruhe Institute of Technology (KIT), 76131 Karlsruhe, Germany; sascha.hasenoehrl@kit.edu (S.H.); julian.peters@kit.edu (J.P.)
* Correspondence: sven.matthiesen@kit.edu; Tel.: +49-721-608-47156

Abstract: As an integral part of a machine, gears are subject to wear, which is influenced by a number of factors. For polymer gears in particular, the uncertainties due to wear are high. These uncertainties outweigh the advantages of polymer gears, such as lower inertia. Improved condition monitoring, for example, with better data acquisition, could reduce these uncertainties and is therefore of great interest. This study addresses the challenges of condition monitoring in polymer gears by investigating the integration of sensors directly onto the gears for improved sensitivity. A compact sensor module mounted on a polymer gear is presented to demonstrate the benefits of integrated sensors. The research compares the effectiveness of integrated acceleration and temperature sensors with state of the art external methods. The results show that the in situ sensor module (ISM) provides reliable measurements for condition monitoring with integrated sensors. A comparative analysis with methods based on the current state of research highlights the increased sensitivity of condition monitoring based on the ISM acceleration sensors compared to traditional bearing block sensors. This increased sensitivity shows a clear advantage of integrated sensors over established methods. The temperature curve of the integrated sensors is sensitive to abrasive wear and gear failure, indicating the wider potential of integrated temperature sensors. In conclusion, this research lays the foundation for advanced condition monitoring using integrated sensors in polymer gears. The knowledge gained contributes to optimising gear applications, promoting cost-effectiveness and aligning with the principles of the Internet of Things and Industry 4.0.

Keywords: in situ; condition; vibration; analysis; smart gear; thermal behavior; damage

Citation: Hasenoehrl, S.; Peters, J.; Matthiesen, S. Integration of Sensors for Enhanced Condition Monitoring in Polymer Gears: A Comparative Study of Acceleration and Temperature Sensors. *Appl. Sci.* **2024**, *14*, 2240. https://doi.org/10.3390/app14062240

Academic Editors: Franco Concli, Aleksandar Miltenovic and Stefan Schumann

Received: 29 January 2024
Revised: 28 February 2024
Accepted: 4 March 2024
Published: 7 March 2024

1. Introduction

Gears are one of the most common used machine elements. The wear of gears is highly dependent on the loads, speed and environment it experiences during its life cycle [1]. The geometric changes in the gears due to wear result in a transmission error, which in turn leads to additional transmission losses and noise [2–4]. If the machine is not properly maintained, this wear can cause gear failure, a loss of function and further damage to the machine [3]. Consequently, wear leads to high costs and long periods of downtime. Therefore, it is more economic to monitor gear wear and detect faults early. In addition, polymer gears are highly susceptible to wear, but they have great potential due to their cost-effectiveness and low mass, resulting in low energy requirements in applications with high acceleration change [5]. Better monitoring of the wear of polymer gears could lead to their wider use, resulting in more cost-effective and environmentally friendly gear applications. To achieve better monitoring, research is needed into more sensitive condition monitoring that can reliably detect mild wear, indicate the degree of wear or even predict the remaining useful life [3,6]. Therefore, two points can be addressed: improve the data acquisition process or improve the analysis methods to resolve the actual wear. This work focuses on the first aspect by exploring integrated sensors in gears, which could enable

more sensitive condition monitoring through new sensor concepts and higher signal quality. In addition, the use of more sensor-integrated machine elements enables better monitoring of machines in general. General machine monitoring can lead to optimisations of various kinds, such as more efficient production lines. Those connected sensors are of great interest in the context of the Internet of Things and Industry 4.0.

1.1. Sensors

The current state-of-the-art method for capturing the data necessary for gear condition monitoring is by using acceleration sensors on the bearing blocks or casing [2,7,8]. The mounting of the sensors means that vibrations are not measured at their source. These measurements are also called ex situ, as opposed to in situ, which means at the source. As a result, the vibration signal contains vibrations from multiple moving elements along the signal path. Furthermore, the longer the signal path, the more dampened the signal gets [2,9,10]. Consequently, the signal quality can be poor, making it difficult to detect mild wear. Chen et al. also emphasized the necessity of monitoring mild wear [6].

However, the approach of integrating sensors into machine elements of the transmission is not new, as several studies show [7,11,12]. In the following, a few such studies are introduced. The design is similar for all of them. The sensors are placed as close as possible to the source of vibration. The sensors are scanned by a central processing unit which temporarily stores or wirelessly transmits the data. Additionally, a power supply module is required. It is not always the case that all of these necessary components are integrated. Smith et al. [11], Lewicki et al. [7] and Peters et al. [12] all presented accelerometers integrated into a gear or a hollow shaft. They showed that it was possible to detect faults like spalling, tooth fracture or heavy wear with in situ measured data. Although Martin et al. suggested an additional benefit from shortening the signal path [9], the benefit could not be demonstrated. This lack of demonstration could be due to poor sensor data as noted by Smith et al. and Peters et al. Lewicki et al. integrated the sensor into a hollow shaft, resulting in a longer signal path than the others. These factors may explain why the quality of condition monitoring was not as good as expected. Another problem is the space required by the solutions presented. Due to the design chosen, the sensors were installed separately from the microcontroller. This design required a second module on the shaft, which takes up extra space. For full integration on the gearwheel, the sensor and the necessary accessories such as microcontroller and data transfer unit need to be even smaller. There are a number of publications dealing with the full integration of sensors into the gearwheel [13,14].

Besides vibration signals, temperature is one of the common quantities which is used for condition monitoring in general [15]. Elforjani et al. used an integrated sensor that measured the temperature of the oil bath. It was shown that it is possible to detect tooth breakage due to higher temperatures [15]. This method is only suitable for measuring temperature where oil bath lubrication is used. The method is not suitable for other types of lubrication such as grease or dry running. In addition, it is not possible to differentiate the fault between several gears in a gearbox. Resendiz-Ochoa et al. conducted a study to classify the abrasive wear of steel gears based on gearbox temperature [16]. Temperature was measured using an infrared camera, and the classification was based solely on features extracted from the camera images. The study did not measure the temperature of individual gears [16]. To overcome the challenge of measuring temperature at individual gears, it would be necessary to integrate the temperature sensor into the gear.

In conclusion, the condition monitoring of gearboxes based on integrated sensors, namely, acceleration sensors, is part of ongoing research. Other sensors with potential, such as temperature sensors, have received less attention. In addition, the benefits of these integrated acceleration sensors have not yet been experimentally proven, although the benefit of integrated sensors, which would be crucial for monitoring mild wear, has been shown in theory.

1.2. Polymer Gears

By integrating sensors, it could be possible to monitor even small changes in gears due to wear. This monitoring is even more important with the increasing use of polymer gears. One of the commonly used polymer materials for gears is polyoxymethylene (POM). POM gears have many advantages over steel gears: low cost, low weight and the ability to run without lubrication [5,17]. However, they have a higher wear rate, which depends on the surface temperature of the gear flank [18,19]. For the reliable operation of POM gears over long lifetimes and potentially critical operating conditions, condition monitoring could help to assess gear performance and predict potential failures. For the overall wear process of POM gears, three phases were found. First, there is a running-in phase, then a linear wear phase and finally a rapid wear phase [18,19]. At higher loads, the first two phases become shorter until they are absent at a certain load. It was shown that POM gears may experience this phenomenon when subjected to loads exceeding 10 Nm at an ambient temperature of approximately 25 °C [18,19]. Apart from abrasive wear, thermal wear is the main wear component for a POM/steel pairing [20]. The wear rate is similar to that of a POM/POM combination [18]. However, the running-in phase tends to be shorter for a POM/steel combination than for a POM/POM combination [21].

In conclusion, POM gears can have an advantage over steel gears and the wear mechanisms can be similar. However, due to a higher wear rate and more complex interdependencies, the disadvantages outweigh the advantages and the use of POM gears remains limited.

1.3. Vibration Analysis

Vibration analysis is an established method to monitor gear condition [22]. It is based on the acceleration of the gear teeth as they mesh. This process gives the Gear Mesh Frequency (GMF), which is very important for analysis, as well as its harmonics [3,6,23]. The GMF is always the same for two mating gears because both gears are mounted on different shafts and the shaft frequency is dependent on the number of teeth of a gear. The GMF and its harmonics are calculated as follows:

$$\begin{gathered} GMF_i = i \cdot f_s \cdot n \\ i: \text{ order of GMF} \\ f_s: \text{ shaft frequency} \\ n: \text{ number of teeth} \end{gathered} \tag{1}$$

As the gear teeth change due to heavy wear or damage, the vibration signals change. This change affects especially the amplitude of the GMF_i [4]. Ziaran et al. suggested that harmonics should be considered at least up to the third order [23]. There are common metrics to detect a fault in gears based on this change in the vibration signal. These metrics are called Gear Condition Metrics (GCMs) and differ in their ability to detect severe faults, monitor faults over time and detect different types of wear mechanisms [24,25].

Two of these metrics have been chosen for this study. The GCMs are calculated as described in Table 1. Table 2 lists the components which are part of the regular, differential and residual vibration signal. More information about the metrics can be found in [24,25].

Table 1. GCMs used in this study.

GCM	Formula		Description
Energy Ratio (ER)	$ER = \frac{\sigma(d)}{\sigma(reg)}$	(2)	$\sigma(d)$: standard deviation of the differential signal of a data sample $\sigma(reg)$: standard deviation of the regular signal of a data sample N: number of data points in a vibration signal res: residual vibration signal res_{OK}: residual vibration signal of a data sample of the unworn gear
$NA4^*$	$NA4^* = \frac{\frac{1}{N}\sum_{i=1}^{N}(res_i - \overline{res})^4}{(var(res_{ok}))^2}$	(3)	

Table 2. Composites of vibration signals.

Signal	Composite
Regular	Shaft frequency and GMF_i plus sidebands up to fourth harmonic
Differential	Normal vibration signal with removed shaft frequency and GMF_i plus sidebands up to fourth harmonic
Residual	Normal vibration signal with removed shaft frequency and GMF_i plus first order sidebands

The effect of different wear patterns on the frequency spectrum was investigated by Ziaran et al. [23] and Amaranth et al. [26]. They found a change in the sidebands of the GMF as the wear progressed from pitting to abrasive. This change shows that the sidebands respond to abrasive wear, which is the main mechanism considered in this work. Cepstrum analysis uses the inverse Fourier transform to find the periodic components of a signal's spectrum, such as sidebands. Formula (4) is used to calculate the real cepstrum, which is used in this paper:

$$\begin{gathered} C_r = \mathcal{F}^{-1}\{\log(|\mathcal{F}\{f(t)\}|)\} \\ C_r: \text{ Cepstrum} \\ f(t): \text{ vibration signal} \end{gathered} \tag{4}$$

Kumar et al. showed that it is possible to detect faults in POM gears using vibration analysis [8]. However, in most cases, it was not possible to distinguish between a healthy gear and pitting on a single tooth using vibration analysis. It should be noted that in some cases, even pitting spread over several teeth indicated an even healthier gear than pitting on a single tooth. The unclear results could be due to the greater damping of non-fibre-reinforced polymers compared to steel [5]. Better monitoring of gears reduces the uncertainty of wear, enabling use in a wider range of applications, the predictive maintenance of machinery and the reuse of gears.

In conclusion, there are several vibration analysis methods for detecting wear with different objectives. It has already been shown that some of these methods can be applied to polymer gears, but the results are difficult to interpret.

1.4. Aim of the Contribution

The state of research shows the need to find a way of collecting wear-correlated data in polymer gears, that provides better data quality. Current methods, such as bearing block sensors, may not be sufficient for detecting wear in polymer gears due to potential high signal damping for ductile polymers. Other methods, such as thermal analysis based on external sensors, are unable to detect faults of individual gears within a gearbox. The approach followed in this contribution is to integrate the sensors onto the gear and measure the variables in situ.

Based on the state of research, the research questions that will be investigated in this contribution are as follows:

Can the integration of sensors into a POM gear lead to better condition monitoring of the gear?

1. Can integrated acceleration sensors provide more sensitive condition monitoring of POM gears than external acceleration sensors?
2. Can integrated temperature sensors into the POM gear provide reliable data that correlate with the wear of the gear?

The aim of this paper is to investigate integrated sensors for the wear condition monitoring of a POM gear.

2. Materials and Methods

The research questions include the following aspects:

- Comparison of state-of-the-art condition monitoring using external acceleration sensors and sensors integrated onto a polymer gearwheel.

- Comparative measurements using a temperature sensor integrated into a polymer gear and correlating the measurement data with the wear of the gear.

A compact sensor module is presented in this paper. This module is equipped with acceleration and temperature sensors and is mounted on a polymer gear. As part of the objective, the benefit of an integrated acceleration sensor over the state-of-the-art bearing block sensors is investigated through an experimental study. The response of an integrated temperature sensor to wear will also be investigated by comparing sensor data with validation measurements and actual wear. This research can provide the basis for new condition monitoring methods based on multiple integrated sensors.

2.1. In Situ Sensor Module

A printed circuit board was developed that incorporates a sensor concept to measure the vibration of the gear in situ. The in situ sensor module (ISM) is shown in Figure 1. It consists of two MEMS acceleration sensors (ADXL1005, Analog Devices, Wilmington, MA, USA) which allow a compact design. More details about the sensors are listed in Table 3. They measure the tangential acceleration on the gear. The sampling rate of these sensors is 16 kHz. In addition, the ISM was fitted with two temperature sensors (TMP1075, Texas Instruments, Dallas, TX, USA). These sensors are connected to copper thermal pads on the underside of the ISM to transfer the heat from the gear. The thermal conductivity of the copper thermal pads is 380 W/m·K. Therefore, the sensors were able to measure the temperature of the gear wheels core surface every 5 min. The ISM is controlled by a microcontroller (STM32WB55RG, ST microelectronics, Geneva, Switzerland). The recorded data is stored in flash memory on the ISM. The storing is due to the sampling rate of the accelerometers, which results in a large amount of measurement data. The microcontroller also allows data to be sent via Bluetooth Low Energy (BLE), which is used to send the data to a host computer for final storage and analysis. The BLE is also used to control the ISM via commands. This control allows data acquisition from the sensors to be started dynamically and with variable measurement durations. In addition, a special command can be used to check the status of the ISM and stop the test bench if an error occurs. All components are mounted directly on the module's circuit board. The circuit board and the microcontroller are powered by two LiPo 120 mAh batteries that are mounted on top of this board using a 3D-printed holder. This design allows the complete ISM to be mounted directly and flush to the gearwheel using screws that pass through the gear, as shown in Figure 1. Without the need for an additional module on the shaft or bearing block, it is more compact than the designs of Smith et al. [11], Lewicki et al. [7] and Peters et al. [12].

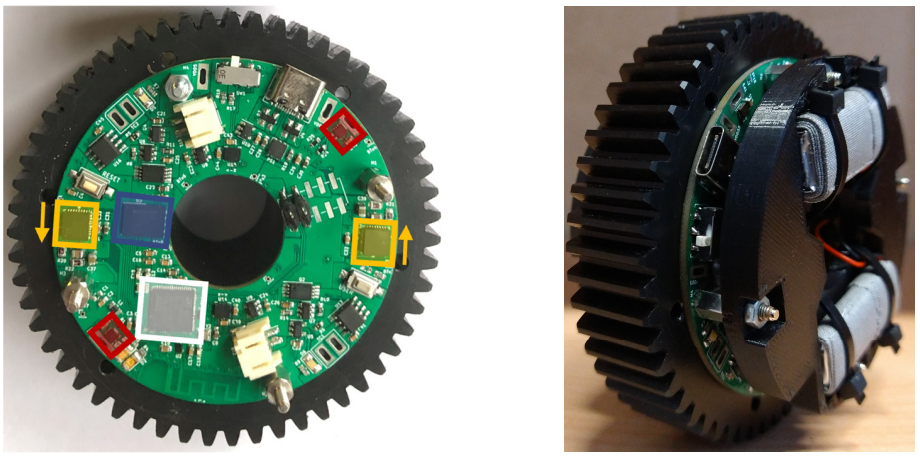

(**a**) (**b**)

Figure 1. Pictures of the ISM on the POM gear: (**a**) without batteries (white: microcontroller; blue: flash memory; yellow: accelerometer and direction of measurement; red: temperature sensor); (**b**) with the battery holder and batteries.

Table 3. Properties of the sensors.

	In Situ Sensor Module (ISM)	Bearing Block Sensors (BBSs)
Name	ADXL05	PCB-356A02
Type	MEMS with analog output	Piezo
Measurement range	±100 g	±50 g
Frequency Range	23 kHz	5 kHz
Resonance Frequency	42 kHz	25 kHz
Sensitivity	14.3 mV/g	10 mV/g
Sensitivity change from 20 °C to 50 °C	±2%	−10–0%
Noise Density	125 µg/√Hz	5 µg/√Hz

2.2. Test Bench Setup

The ISM was mounted directly onto POM gears (Mädler, Stuttgart, Germany). The characteristics of the gears are given in Table 4. The POM gears were fixed to the shaft with a locking assembly. According to the manufacturer, these gears can run at a continuous temperature of up to 100 °C. A steel gear was selected as the mating gear. This selection is a common material paring for gears [20,27]. The material paring results in lower temperatures on the POM gear, which is desired to control the wear rate [21]. For more information on the gears, see Table 4. No lubrication was added to the setup, which is a common mode of operation for polymer gears [27]. The width of the steel gear is smaller than that of the POM gear. This difference means that not the whole POM gear is engaged. The smaller engagement area helps to accelerate the wear progress. Two synchronous motors were selected for the drive and load (CMP71L, SEW-Eurodrive, Bruchsal, Germany). Two piezo sensors (PCB-356A02, PCB Piezotronics, Depew, NY, USA) were mounted on the bearing blocks as a reference measuring system. These sensors will be referred to as Bearing Block Sensors (BBSs). Further information on the piezo sensor is given in Table 3. The test bench configuration is shown in Figure 2. An ADwin Pro II with a T11 CPU was used to record the data and control the test procedure described in Section 2.3.

Table 4. Properties of the gears.

	POM Gear	Steel Gear
Material	POM	steel
Fabrication	milled	milled
Module	1.5	1.5
Number of teeth	55	65
Width	17 mm	10 mm
Diameter	82.5 mm	97.5 mm
Weight	165 g	742 g
Thermal conductivity	0.31 W/m·K	50.2 W/m·K

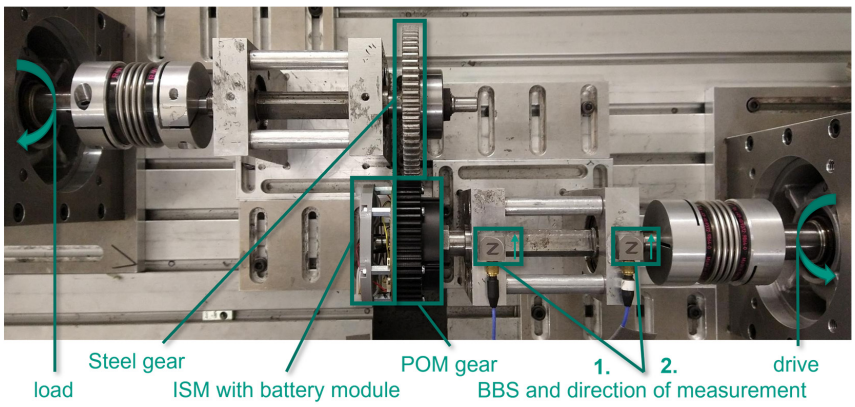

Figure 2. Configuration of the test bench.

2.3. Test Procedure

For the study in this paper, two POM gears were fitted with an ISM and run alternately on the test bench. In the following, these are called gear 1 and gear 2. The BBSs were used to compare the in situ data with the conventional method of recording vibration data. The sampling rate of the piezo sensors was 10 kHz. The drive ran at a constant 1000 rpm, which is a shaft frequency of 16.7 Hz, and the load was a constant 10 Nm. An overview of the main frequencies is given in Table 5. Both the ISM and the BBSs collected data synchronously for 1 min every 20 min. The test bench was stopped after running for two hours to measure the actual wear and recharge the batteries. These two hours are referred to as two-hour sequences in the following. They consist of 1.2×10^5 cycles of the polymer gear. After recharging, the gears were remounted and the next two-hour sequence began. Figure 3 displays the flow of the test procedure. Additionally, a 1 min acceleration sample was taken at the beginning of the tests to provide a comparison with the acceleration signal of a completely healthy gear.

Table 5. Shaft frequency and GMF_i up to the fourth order.

Shaft Frequency	GMF_1	GMF_2	GMF_3	GMF_4
16.7 Hz	916.7 Hz	1833.3 Hz	2750 Hz	3666.7 Hz

Figure 3. Flow of the test procedure.

Polymer gears have a risk of melting at elevated temperatures. The melting would lead to a very fast and abrupt failure. To ensure progressive wear, the temperature had to be below the melting temperature. To confirm that this temperature was not reached in the study, the surface temperature of the loaded flanks of gear 1 was measured. The measurement was also performed to validate the measurements of the integrated temperature sensors on the ISM. The temperature was measured for the second two-hour sequence beginning from 2 h running time. During this period, the temperature was measured every 5 min until a steady-state tooth surface temperature was reached at 3:40 h. The temperature comparison measurements were made using a handheld infrared camera (FLIR E6, FLIR Systems Inc., Wilsonville, OR, USA).

Because of the complex relationship between the vibration signal and wear, it was also necessary to measure the actual wear. For this study, the normed wear was defined as the difference between the measured value and the initial value. To quantify it, the mass loss and the loss of Lateral Surface Area (LSA) was measured. Therefore, the weight of the POM gears was measured using a scale with a precision of ±0.0004 g (PCE-ABI 220, PCE Deutschland GmbH, Meschede, Germany). The ISM and battery holder were not removed as their weight remained the same. Weighting is a common method for measuring wear [12,28]. The LSA was measured using a digital microscope (VHX2000, Keyence, Osaka, Japan). A similar method was used by Mao et al. who measured the tooth width [29]. The LSA was measured for two different teeth on each POM gear.

2.4. Data Processing

Prior to vibration analysis, the in situ data were down-sampled from 16 kHz to 10 kHz. The down-sampling was performed to improve the comparability of the in situ data with

the ex-situ data. The aim was to obtain the GMF up to the fourth order, which corresponds to 3.7 kHz. Therefore, 10 kHz is sufficient to satisfy Shannon's sampling theorem [30]. All data were then filtered with a sixth-order Butterworth bandpass. As the fourth-order GMF should be preserved, 4 kHz was used as the upper bound. The lower bound was set to 5 Hz. For the BBS, the tangential measurement direction shown in Figure 2 was used for comparison. The maximum amplitude of each two-hour sequence vibration signal, spectrum, cepstrum and GMCs were then calculated. From Section 2.3, the NA4* metric has an N of 600,000 and the residual of the first 1 min sample was assumed to be r_{OK}. The average of the two MEMS sensors on the ISMs and the two BBSs was taken. The results were then compared. The normed wear was calculated by dividing the mass and LSA loss by their respective maximum values. The temperature measurements were used to calculate the static difference temperature by subtracting the ambient temperature from the gear maximum temperature. To determine the increased sensitivity, the quotient of the GCM of the BBS and the ISM was calculated.

3. Results

Gear 1 ran for 15.6×10^5 cycles without a total loss of function. However, the shaft-hub connection of gear 2 showed server damage after 6.8×10^5 cycles of running, so data analysis was only possible up to that point. The results of this data analysis are presented in the following section, starting with wear, then temperature and finally vibration.

3.1. Wear

A picture of the melted inner radius of gear 2 is shown in Figure 4. Figure 5a,b are digital microscope images of gear 1. They show the shrunken Lateral Surface Area (LSA) of the new gear 1 against the worn gear 1. The left side of the LSA in Figure 5b shows that not only is the tooth getting smaller as indicated by the measured area, but the material is also being displaced. Weight measurements taken to monitor the wear of the POM gears are shown in Figure 6a. The weight of gear 1 is higher than that of gear 2 due to a different design of the battery holder. Over the course of the study, the weight of both gears decreases in all measurements. Initially, the decrease is slightly steeper for gear 2 than for gear 1. The LSA shown in Figure 6b decreases overall with a very similar slope for gear 1 and gear 2. There is also an increase from time to time; this phenomenon will be discussed in Section 4.1. Overall, the LSA of tooth 2 of gear 1 decreases slightly faster than the LSA of tooth 1. As can be seen from the approximation of the normed wear in Figure 6c, the loss of weight and LSA of the POM gear has the same linear trend.

Figure 4. Molten shaft hub connection of gear 2 after failure.

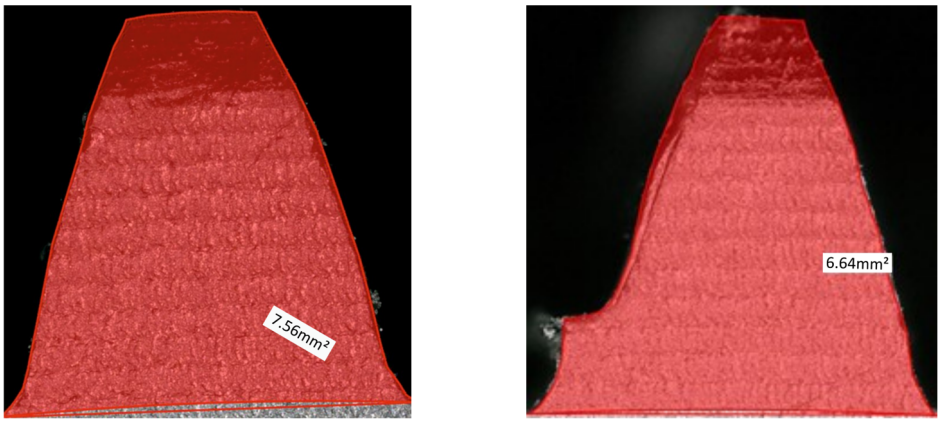

Figure 5. LSA 1 of gear 1: (**a**) after 0 cycles; (**b**) after 15.6 × 10^5 cycles.

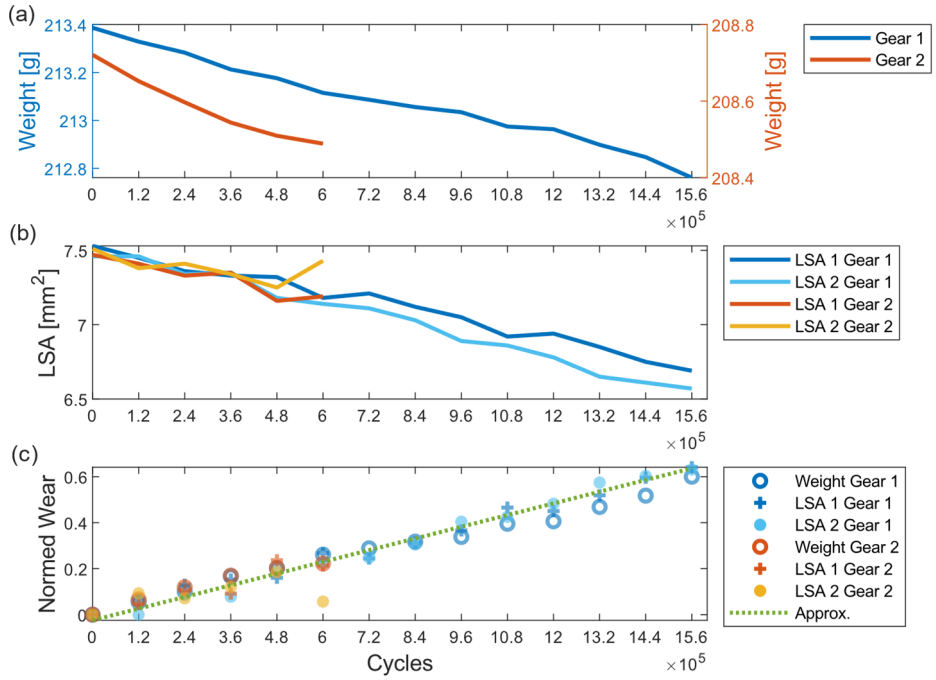

Figure 6. Wear of the POM gears: (**a**) weight of the gear plus ISM and battery holder; (**b**) LSA; (**c**) normed wear.

3.2. Temperature

Figure 7 shows the temperature over a two-hour sequence. The sequences all look similar, apart from the failure sequence. The temperature followed a bounded growth. Both the reference measurement of the infrared camera and that of gear 1 from 2 h to 3:40 h start at roughly the same room temperature of 22 °C and increase over the sequence. The bound is at about 41 °C and was reached at about 1:20 h into the two-hour sequence. The progression of the temperature curve measured using the ISM at the same time follows the progression of the temperature measured using the infrared camera. This progression also counts for the second temperature curve of gear 1 shown in Figure 7. For gear 2, the temperature measured using the ISM is shown for the two-hour sequence in which the shaft–hub connection failed. The temperature rises more steeply from the beginning, but still follows a bounded growth until 1 h. However, after 1 h of operation, the temperature starts to rise steeply. It reaches a peak at the failure time of 11:20 h of running.

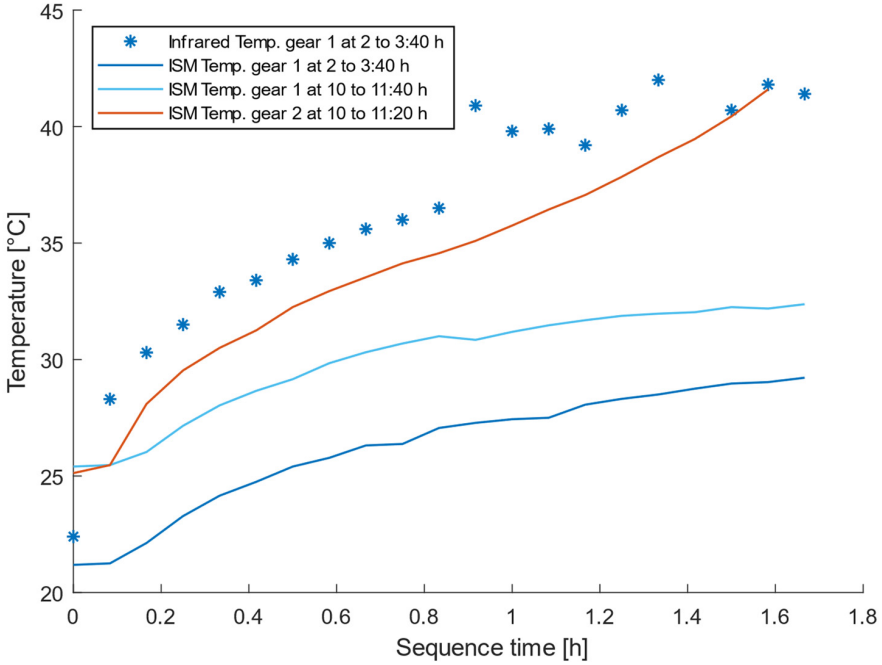

Figure 7. Temperature of gear 1 between 2 and 3:40 h running time and gear 1 and 2 between 10 and 11:40 and 11:20 h respectively.

Figure 8 shows the maximum and static difference temperature of each two-hour sequence measured using the ISM. At the beginning, the maximum temperature of both gears increases. This increase applies to both the absolute and the static difference temperature. For the maximum temperature, the increase is about 17%. The static difference temperature increases by about 100%. Then, the static difference temperature decreases by about 50%. The static difference temperature of gear 1 then remains almost constant. In contrast, the shaft hub connection of gear 2 fails and the temperature rises to 42 °C.

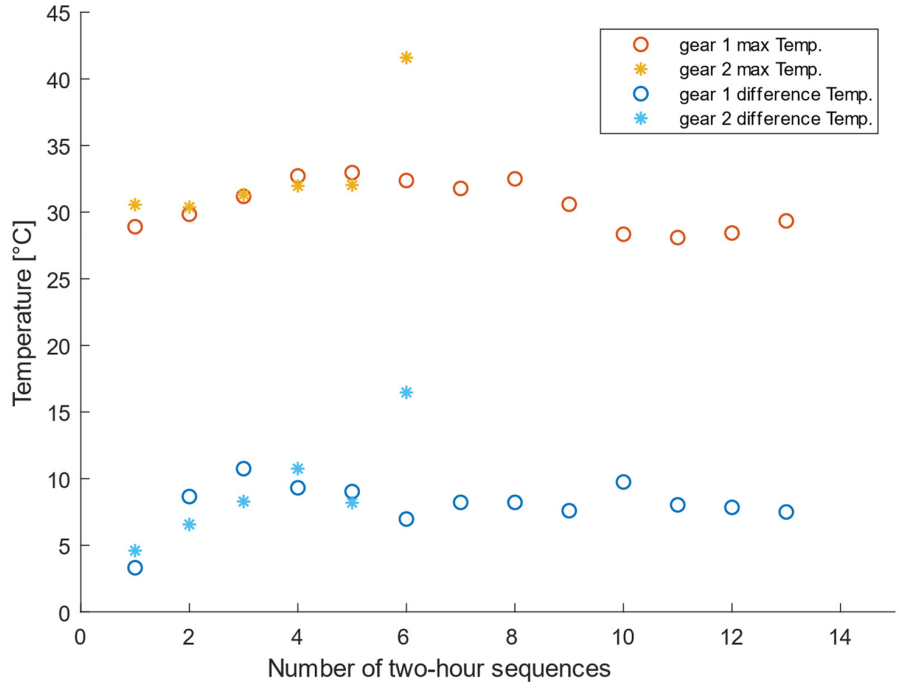

Figure 8. Maximum and static difference temperature measured using the ISM of gear 1 and gear 2 over every two-hour sequence.

3.3. Acceleration Signal Properties

Figure 9 shows the effect of wear on the acceleration spectrum. The shaft frequency is clearly visible in Figure 9a; GMF_1 and GMF_2 are visible in Figure 9a,b and all at the frequencies shown in Table 5. The shaft frequency dominates the spectrum of the ISM. However, with BBS, the shaft frequency is low. GMF_1 is the dominant frequency. For both sensors, GMF_2 is still visible. The amplitude of the higher GMF_i is too low compared to the rest of the spectrum to be visible. As wear progresses, the lower frequencies under 2 kHz increase the most. GMF_1 and its sidebands almost double after 2×10^5 cycles for the ISM. The sidebands reach almost half the intensity of the GMF. For the BBS, the increase of the GMF_1 is even greater. However, the sidebands are less than half of the GMF_1. Therefore, the sidebands relative to the GMF_1 of the BBS are smaller than those of the ISM. In addition, two harmonics increase between the shaft frequency and the GMF_1 at frequencies of 366.7 Hz and 550 Hz. The further increase up to 15.6×10^5 cycles of the GMF_i and their sidebands is very small. Instead, the harmonics between the shaft frequency and the GMF_1, which first increased, have now shifted from 366.7 Hz and 550 Hz to 200 Hz and 716.7 Hz, respectively. For both sensor types, it appears that the first GMF increases with wear but the second decreases. The amplitude of the measured acceleration by the ISM is generally much lower compared to the amplitude of the BBS. In the case of GMF_1 and GMF_2, the amplitudes of the ISM are about one tenth of the amplitudes of the two GMF_i for the BBS.

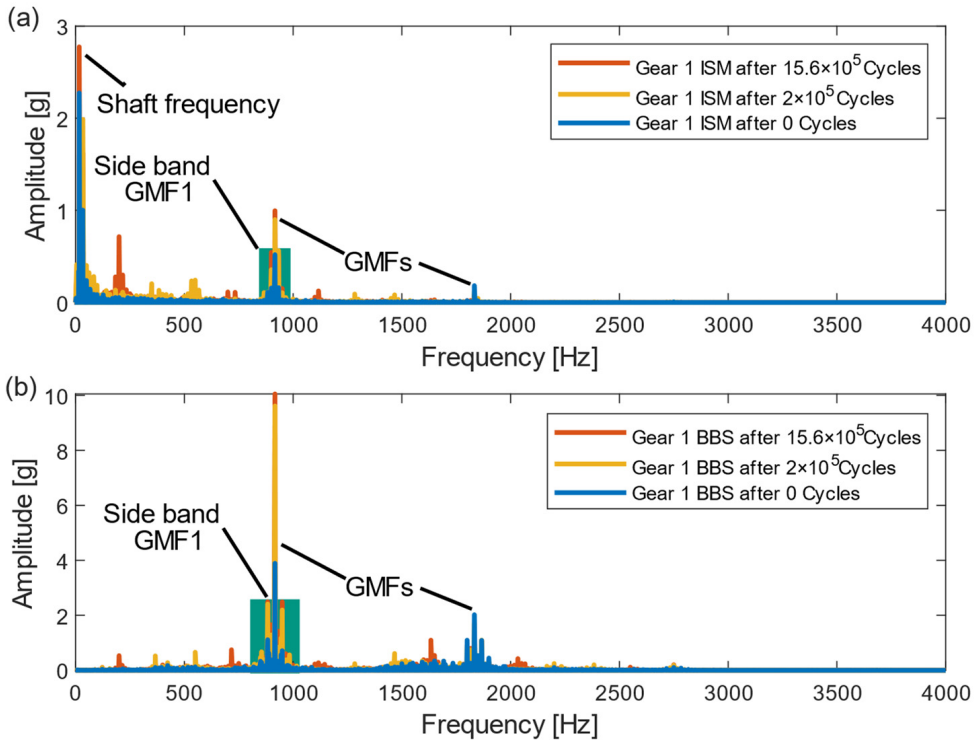

Figure 9. Acceleration spectrum of gear 1: (**a**) ISM; (**b**) BBS.

An analysis of the amplitude of the GMF_1 confirms these findings. Figure 10 shows that the acceleration amplitude at the GMF_1 at 916.7 Hz increases for both gears and both sensor types (ISM, BBS). It shows that there are two phases. Up to about 2×10^5 cycles, the amplitude increases steeply. After that, the amplitude remains approximately constant for the BBS. However, the amplitude of the ISM drops at the start of several two-hour sequences. This drop does not appear in the amplitude of the cepstrum which represents the sidebands. The amplitude of the ISM GMF_1 is about a factor of 10 lower than the amplitudes of the BBS GMF_1.

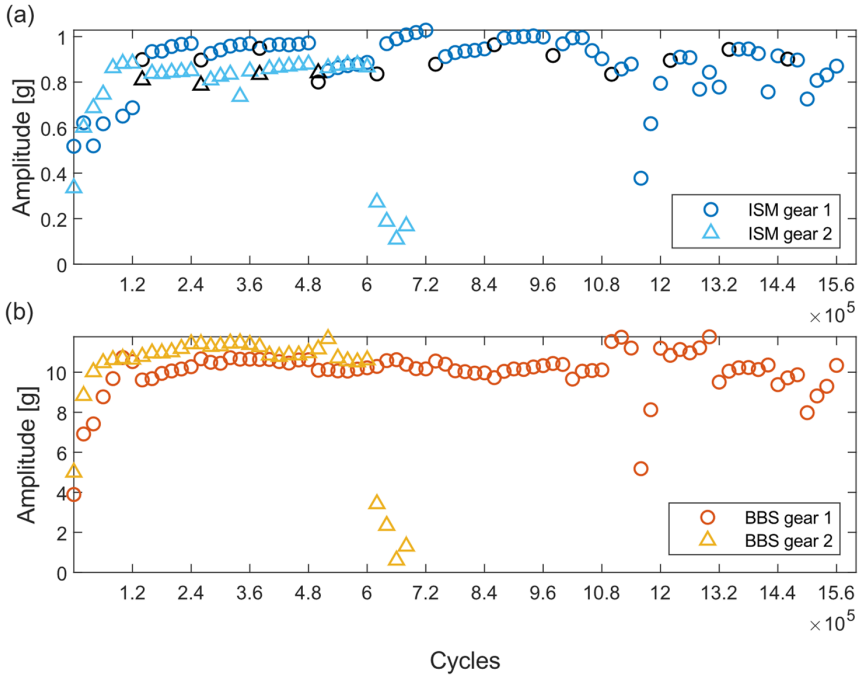

Figure 10. Amplitude of the spectrum of the first GMF: (**a**) ISM with the beginning of each two-hour sequence marked in black; (**b**) BBS.

Figure 11 shows that the cepstrum of the GMF_1 decreases first. After this first phase, the cepstrum starts to fluctuate and slowly decreases. The amplitudes of the ISM sideband are about a factor of 2 lower than the amplitudes of the BBS sideband. Therefore, the relative height of the sidebands to the GMFs is higher for the ISM than for the BBS. The failure of gear 2 is clearly visible as the amplitude of the GMF_1 rapidly decreases and the amplitude of the sideband rises. Figure 12 shows the maximum amplitudes of the vibration signal. It can be observed that the amplitudes measured using the BBS are much higher. Due to an error while saving the data, the ISM data for gear 1 are missing from 0.6×10^5 to 1×10^5 cycles in Figures 10a, 11a and 12.

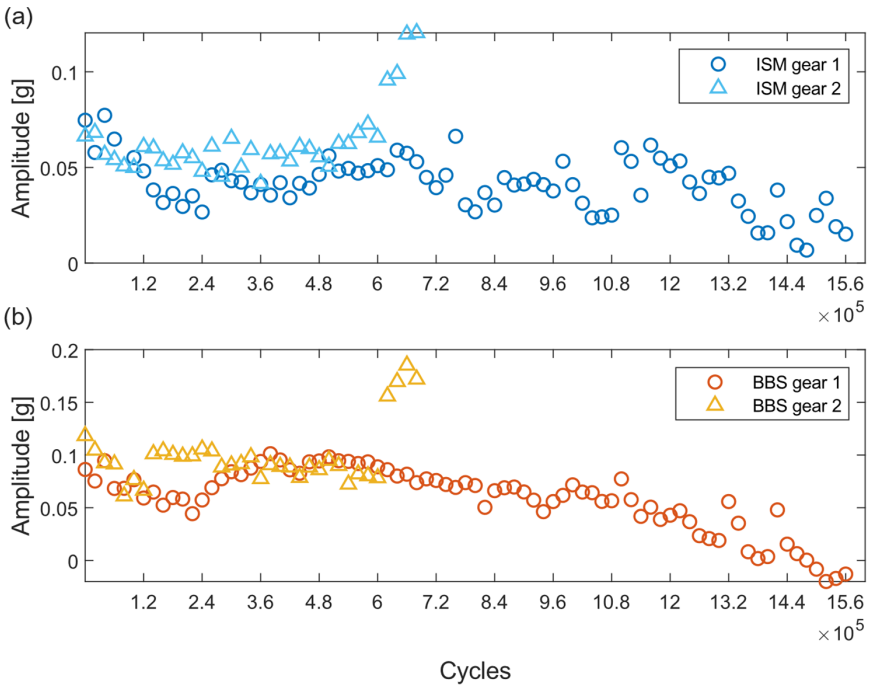

Figure 11. Amplitude of the cepstrum of the first GMF: (**a**) ISM; (**b**) BBS.

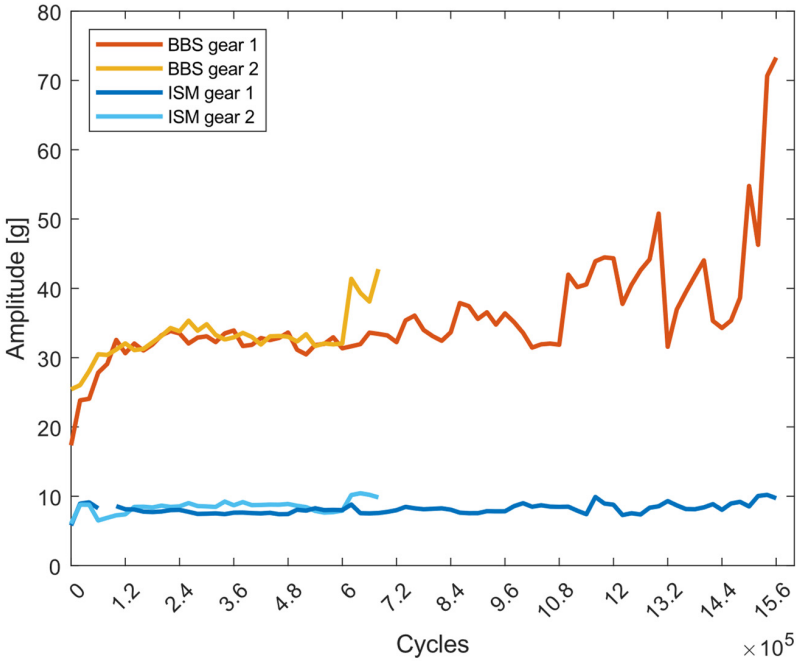

Figure 12. Maximum amplitude of each two-hour vibration signal.

3.4. Gear Condition Metrics

Figures 13 and 14 show the calculated GCMs normed to their maximum values. There are three phases identified for both GCMs. The first phase is an increase or decrease in the metrics. This phase is followed by a phase of almost constant values. The last phase is an overall increase in the GCMs. In the first phase, the ER acts inversely on the ISM and BBS. The ISM increases and the BBS decreases. An exception to that is the last measurement point in the first phase of gear 2 which is decreasing. The increase of the third phase in the ER starts steeper for the ISM. At this phase, the ER of the ISM is on average 81% higher than that of the BBS.

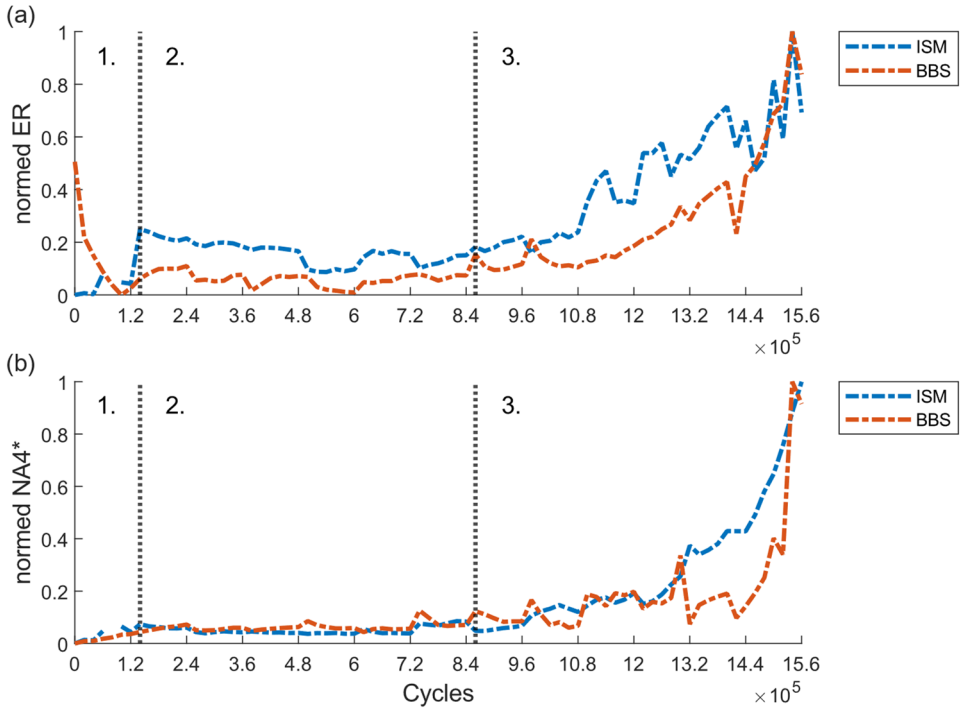

Figure 13. GCMs of gear 1 with a separation of the three phases: (**a**) ER; (**b**) NA4*.

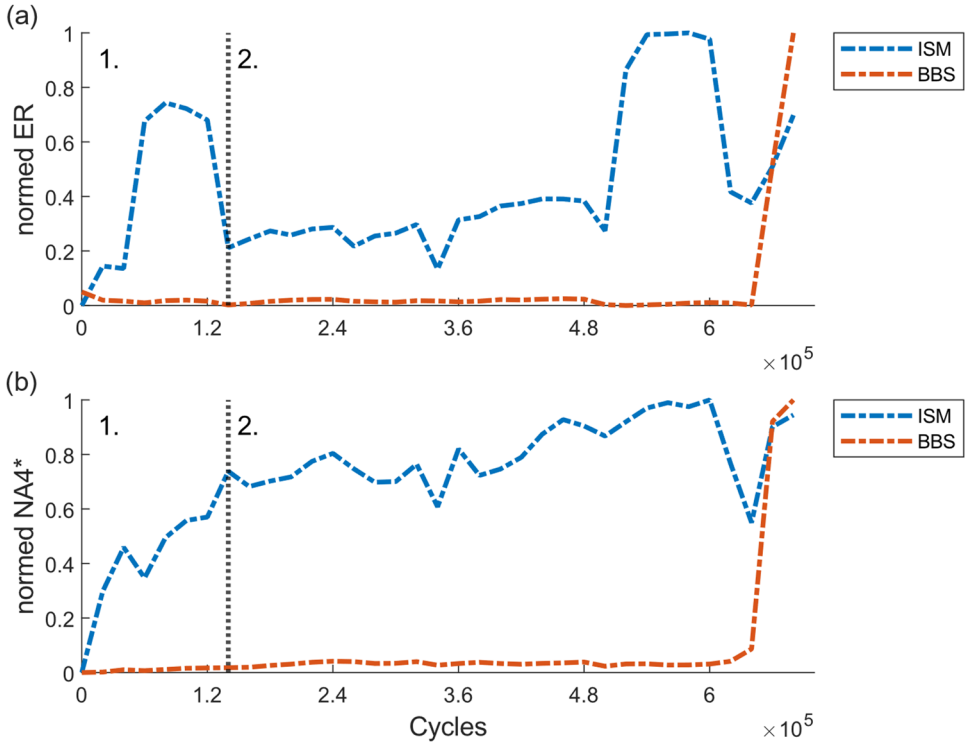

Figure 14. GCMs of gear 2 with a separation of the two phases: (**a**) ER; (**b**) NA4*.

In the first phase, the NA4* increases for both sensors. The third phase of the NA4* is similar to that of the ER, with a steeper slope. The NA4* of the BBS is fluctuating much more than the ISM. Due to these fluctuations, the increase of the BBS and ISM seems to be similar in the beginning, but leading to an earlier and more significant increase of the metric for the ISM later into the phase. For the third phase, the NA4* of the ISM is on average about 56% higher than that of the BBS.

In the second and third phases, the GCMs fluctuate strongly at the beginning of a two-hour sequence. These are only visible in the BBS signal. Overall, the NA4* for the ISM is the smoothest. The first two phases appear for both gears. The third phase is not present in the GCMs of gear 2 since it failed before reaching it. The effect of the failure of the second gear shaft-hub connection first causes a steep decrease for the GCMs of the ISM and then an increase. However, the defect is clearly visible by a steep increase in the GCMs of the BBS. The measurement data for cycle 0.6×10^5 to 1×10^5 from gear 1 are also missing in the GCMs.

4. Discussion

4.1. Wear

There was only a slight difference between the two measurements of wear presented in Section 3.1. The slightly steeper decrease in the weight of gear 2 could be due to manufacturing tolerances. As this effect was not found in the LSA measurements, it is more likely to be due to a measurement uncertainty. A possible cause could be that the gears were not properly cleaned prior to measurement and therefore the difference occurred. However, it is noticeable that the Lateral Surface Areas (LSA) of the teeth increased from time to time. This increase was due to the displacement of the material mentioned above. The displacement made it difficult to define the unworn LSA. Otherwise, the wear behaviours of the LSA and the weight were linear and very similar, suggesting that the wear rate was constant.

No running-in phase or constant wear phase was found due to this constant wear rate. The absence is in line with current research, which indicates that the phases are not present beyond 10 Nm at an ambient temperature of approximately between 20 °C and

25 °C [18,19]. The method of measuring wear using the LSA could possibly be improved by using the average tooth width over the worn surface of the teeth. However, as the LSA and weight give similar results and the aim of the study was not to model wear from the measurements, the methods were good enough. Also, the maximum gear temperature recommended by the manufacturer was not exceeded, as shown by the tooth surface temperature measured using the infrared camera. This temperature means that no melting of the gear teeth occurred. A slightly higher wear rate of the LSA of tooth 2 was observed compared to the LSA of tooth 1 of gear 1. Wear is able to spread from teeth with high wear rate to others. This wear rate means that tooth 2 or one of the surrounding teeth of gear 1 could have a small defect.

4.2. Temperature Sensor

The temperature of the polymer gear reaches an almost static bound temperature after about 1:20 h into a two-hour sequence. This temperature rise is related to the heat flow that is generated by friction in the contact of the gears, which causes the rise of temperature to the static bound temperature on the flanks of the POM gear of approximately 41 °C. Due to the low thermal conductivity of the gear, a temperature rise also takes place at the measurement point of the ISM, but with a delay and a smaller amplitude. The temperature measured using the ISM on the gear body correlates with the temperature measured using the infrared camera on the tooth flanks. This correlation means that although the temperature values measured using the ISM are lower than the flank temperature, the ISM provides reliable temperature data from which conclusions can be drawn about the tooth flank temperature.

The maximum temperature measured using the ISM was always well below the 100 °C specified by the gear manufacturer. This temperature means that the operating point of the gears was never temperature-critical. The relationship between the static difference temperature curve with its two phases as shown in Figure 8 and the linear wear curve of the POM gear in Figure 6 is not linear. Comparing the evolution of the static difference temperature over time (Figure 8) with the curves of the GMF_1 signal characteristics (Figures 9–11), correlations with the temperature curve can be seen. In the first two identified phases of increase in the GMFs and sidebands, the temperature also increases. With the transition to the third phase, the increase in the amplitude of the remaining frequency band, the static differential temperature begins to slowly decrease. This similarity confirms that, similar to Resendiz-Ochoa et al., temperature also has an influence on abrasive wear. Ziaran et al. mapped the different phases of the signal properties to different wear mechanisms [23]. This could mean that the different temperature phases also indicate different wear mechanisms, which causes different friction and therefore different temperatures.

Regarding research question 2 on the integrated temperature sensor, it can be said that the sensor can provide reliable data that correlate with the wear of the POM gear. This correlation is complex and requires further investigation to extract the actual wear condition from the temperature data.

4.3. Vibration Analysis

Section 3.3 described how the spectrum of the ISM is dominated by a lower frequency, such as the shaft frequency. In contrast to that, those frequencies are barely visible for the BBS. One aspect of the domination of the ISM by the shaft frequency is due to the rotating coordinate system of the ISM accelerometers within the Earth's gravitational field. The second aspect is the movement of the accelerometer relative to the mesh position of the gear teeth, which causes a change in the signal path of the vibration and therefore a change in the damping of the signal. Both of these movements occur at the shaft frequency, resulting in a high content of the shaft frequency in the ISM spectrum. As the BBS does not move in relation to the earth's gravity or the mesh position of the gears, the content of the shaft frequency in the spectrum is much lower. This phenomenon was also found by Lewicki et al. The signal properties and the GCM do not show the same linear behavior

as the wear. This discrepancy shows the complex relationship between the wear and the vibration signal. The results of the vibration analysis can be divided into three phases. These phases are visible in the spectrum shown in Section 3.3 and also in the GCMs. The first phase is accruing because of the changes in the GMF and their sidebands. In the second phase, the changes in the vibration signal are too small to have an impact on the GCMs. The last phase is based on an increase in the amplitudes of frequencies between the GMF_i values. Those are part of the differential and the residual signal, which is why the Energy Ratio (ER) and NA4* are increasing.

The increase in GCMs of the ISM in the third phase started earlier and steeper than that of the BBS. This earlier increase emphasizes that the ISM is more sensitive to changes in the gear than the BBS. In the third phase, the sensitivity of the ISM to the measured wear was on average 81% higher for the ER and 56% higher for the NA4*. This higher sensitivity could be due to the shorter signal path resulting in a less damped vibration signal. In Section 3.3, it was shown that the amplitudes of the sidebands relative to the GMF_i of the BBS are much smaller than those of the ISM. These lower sidebands are another sign of the strong dampening effect of the signal path and better signal quality of the ISM. In addition, the longer signal path leads to more interference from other vibrations. These would mainly affect the differential signal. As a result, the NA4* of the BBS fluctuates more. This fluctuation makes the interpretation of the data more difficult. As a result, fault detection may be more robust with the GCMs based on the vibration data measured with the ISM.

The observed higher amplitudes measured using the BBS contradict the idea that the ISM is more sensitive. However, the amplitudes measured are so high that they are not very plausible. As the characteristics of the sensors have been chosen to suit the described application and there is experience of these sensors in other applications, it is assumed that the fault is in the setup. With the BBS, this fault could be the amplifier or the supply voltage. With the ISM, this fault could be the layout of the components or the power consumption. Furthermore, the comparison between the ISM and the BBS was made on a relative basis, so the absolute values do not contradict the results. The reason for the higher amplitudes of the BBS could not be found.

As shown, the phases identified in the vibration signals do not correlate to the wear rate. Ziaran et al. mapped the different phases of the signal properties to different wear mechanisms [23]. Different wear mechanisms could also be the reason for the different phases found in this study. A hint gives the maximum temperature at each two-hour sequence. Since it is increasing along the first phase identified in the vibration signal, this could mean that in this phase, a more temperature-dependent wear mechanism is present. Evidence for the presence of this mechanism cannot be provided, because no wear mechanisms were reviewed in this study.

In Section 3.3, it was described that the GMF_1 drops at the beginning of most of the two-hour sequences. This drop is about 0.1 g out of about 1 g, or about 10%. The temperature change in the ISM over a two-hour sequence is in the range of 20 °C to 50 °C, which can have a total effect on the sensitivity of the acceleration sensors on the ISM of about 4%. As the PCB material is a good thermal insulator, the temperature range and sensitivity deviation should be even smaller. This effect means that the deviation of the GMF_1 at the beginning of each two-hour sequence is not necessarily caused by the change in sensitivity due to temperature, but it may be part of the cause. As described in Section 2.2, the POM gears did not run on their whole tooth surface. Figure 15 shows the resulting half-worn tooth surface. To measure wear, the gears had to be removed after each two-hour sequence. When reinstalled, the position of the gears slightly changed axially. Therefore, the gears ran on a partially unworn tooth surface at the beginning of some two-hour sequences. This change in surface could be another possible reason for the drops in GMF_1.

Regarding research question 1 on the integrated acceleration sensors, it can be said that the vibration analysis based on the ISM provides more sensitive condition monitoring than the BBS. The higher sensitivity may allow milder wear to be monitored more reliably, which is the first step towards better monitoring of the wear condition of POM gears.

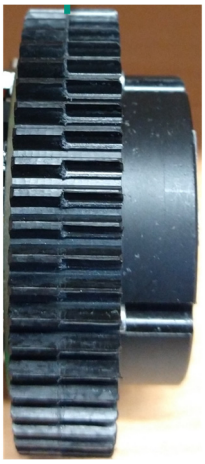

Figure 15. Tooth surface of the worn POM gear 1.

5. Conclusions

This study investigated the sensitivity of the ISM for abrasive condition monitoring on POM gears and explored the added benefit of integrated temperature and acceleration sensors.

The analysis of wear patterns revealed a consistent linear trend, indicating a constant rate of wear. It was concluded that there were no distinct running-in or constant wear phases, aligning with current research suggesting the absence of such phases at ambient temperatures and high loads. The integrated temperature sensors demonstrated the ability to reliably measure gear temperature. The temperature analysis showed bounded growth, reaching a static bound temperature after 1:20 h into a two-hour sequence. The correlation between ISM and infrared camera measurements confirmed the reliability of the ISM temperature data. The increase of the temperature, along with the sidebands, suggested a possible temperature-dependent influence on abrasive wear. A vibration analysis using the ISM highlighted its sensitivity to changes in gear conditions. The dominant presence of lower frequencies, such as the shaft frequency, in the ISM spectrum distinguished it from BBS. Three phases were identified in the GCMs. The ISM showed less variation and higher sensitivity in the results compared to the BBS, indicating the increased robustness of gear condition monitoring. This publication also discussed the potential influence of temperature on ISM accelerometers, which should be considered in future studies.

This study addresses two detailed research questions. Firstly, the study confirms that the vibration analysis based on ISM provides more sensitive condition monitoring, allowing a potentially better assessment of POM gear wear conditions compared to BBS. Secondly, the integrated temperature sensor as part of the ISM provides reliable data that correlate with POM gear wear. Temperature variations over time are consistent with wear characteristics, highlighting the potential of the sensor to assess gear condition.

While this study focused on a high rate of abrasive wear, future research should investigate different wear mechanisms, especially tooth root fracture, which is of high interest. Therefore, the potential benefits of new integrated sensors need to be further explored to improve condition monitoring. Additionally, new models for assessing actual wear based on new integrated sensors must be investigated to achieve better wear monitoring and potentially calculate the remaining useful life of a POM gear. To better understand the uncertainties that come with such wear monitoring based on integrated sensor data and a model, a higher sample size should be investigated in the future.

Author Contributions: Conceptualization, J.P.; methodology, S.H.; software, S.H.; validation, S.H.; formal analysis, S.H.; investigation, S.H.; resources, S.M.; data curation, S.H.; writing—original draft preparation, S.H.; writing—review and editing, J.P.; visualization, S.H.; supervision, S.M.; project administration, S.M.; funding acquisition, S.M. All authors have read and agreed to the published version of the manuscript.

Funding: This research was funded by Dr.-Ing Willy-Höfler-Stiftung. The APC was funded by KIT-Publikationsfonds.

Institutional Review Board Statement: Not applicable.

Informed Consent Statement: Not applicable.

Data Availability Statement: The data that support the findings of this study are available from the corresponding author upon reasonable request.

Conflicts of Interest: The authors declare no conflicts of interest.

Abbreviations

Term	Abbreviation
Polyoxymethylene	POM
Gear Mesh Frequency	GMF
Gear Condition Metrics	GCMs
Energy Ratio	ER
In situ Sensor Module	ISM
Bluetooth Low Energy	BLE
Bearing Block Sensors	BBSs
Lateral Surface Area	LSA

References

1. Eyre, T.S. Wear characteristics of metals. *Tribol. Int.* **1976**, *9*, 203–212. [CrossRef]
2. Smith, J.D. *Gear Noise and Vibration*, 2nd ed.; Review and Expanded; Marcel Dekker: New York, NY, USA; Basel, Switzerland, 2003; ISBN 0-8247-4129-3.
3. Feng, K.; Ji, J.C.; Ni, Q.; Beer, M. A review of vibration-based gear wear monitoring and prediction techniques. *Mech. Syst. Signal Process.* **2023**, *182*, 109605. [CrossRef]
4. Kuang, J.H.; Lin, A.D. The Effect of Tooth Wear on the Vibration Spectrum of a Spur Gear Pair. *J. Vib. Acoust.* **2001**, *123*, 311–317. [CrossRef]
5. Mott, R.L.; Vavrek, E.M.; Wang, J. *Machine Elements in Mechanical Design*, 6th ed.; Pearson Education: New York, NY, USA, 2018; ISBN 978-0-13-444118-4.
6. Chen, X.; Wang, S.; Qiao, B.; Chen, Q. Basic research on machinery fault diagnostics: Past, present, and future trends. *Front. Mech. Eng.* **2018**, *13*, 264–291. [CrossRef]
7. Lewicki, D.; Lambert, N.A.; Wagoner, R.S. *Evaluation of MEMS-Based Wireless Accelerometer Sensors in Detecting Gear Tooth Faults in Helicopter Transmissions*; NASA: Washington, DC, USA, 2015.
8. Kumar, A.; Parey, A.; Kankar, P.K. Vibration based fault detection of polymer gear. *Mater. Today Proc.* **2021**, *44*, 2116–2120. [CrossRef]
9. Martin, G.; Vogel, S.; Schirra, T.; Vorwerk-Handing, G.; Kirchner, E. Methodical Evaluation of Sensor Positions for Condition Monitoring of Gears. In *NordDesign 2018 Proceedings of the NordDesign 2018, Linköping, Sweden, 14–17August 2018*; Ekströmer, P., Schütte, S., Ölvander, J., Eds.; The Design Society: Glasgow, UK, 2018; ISBN 978-91-7685-185-2.
10. Chin, Z.Y.; Borghesani, P.; Smith, W.A.; Randall, R.B.; Peng, Z. Monitoring gear wear with transmission error. *Wear* **2023**, *523*, 204803. [CrossRef]
11. Smith, W.; Deshpande, L.; Randall, R.; Li, H. Gear diagnostics in a planetary gearbox: A study using internal and external vibration signals. *Int J Cond. Monit.* **2013**, *3*, 36–41. [CrossRef]
12. Peters, J.; Ott, L.; Dörr, M.; Gwosch, T.; Matthiesen, S. Sensor-integrating gears: Wear detection by in-situ MEMS acceleration sensors. *Forsch. Ingenieurwes* **2021**, *86*, 421–432. [CrossRef]
13. Binder, M.; Stapff, V.; Heinig, A.; Schmitt, M.; Seidel, C.; Reinhart, G. Additive manufacturing of a passive, sensor-monitored 16MnCr5 steel gear incorporating a wireless signal transmission system. *Procedia CIRP* **2022**, *107*, 505–510. [CrossRef]
14. Bonaiti, L.; Knoll, E.; Otto, M.; Gorla, C.; Stahl, K. The Effect of Sensor Integration on the Load Carrying Capacity of Gears. *Machines* **2022**, *10*, 888. [CrossRef]
15. Elforjani, B.; Xu, Y.; Brethee, K.; Wu, Z.; Gu, F.; Ball, A. Monitoring gearbox using a wireless temperature node powered by thermal energy harvesting module. In Proceedings of the 23rd International Conference on Automation and Computing (ICAC), Huddersfield, UK, 7–8 September 2017; pp. 1–6. [CrossRef]
16. Resendiz-Ochoa, E.; Saucedo-Dorantes, J.J.; Benitez-Rangel, J.P.; Osornio-Rios, R.A.; Morales-Hernandez, L.A. Novel Methodology for Condition Monitoring of Gear Wear Using Supervised Learning and Infrared Thermography. *Appl. Sci.* **2020**, *10*, 506. [CrossRef]
17. Alharbi, K.A.M. Wear and Mechanical Contact Behavior of Polymer Gears. *J. Tribol.* **2019**, *141*, 011101. [CrossRef]

18. Hooke, C.J.; Mao, K.; Walton, D.; Breeds, A.R.; Kukureka, S.N. Measurement and Prediction of the Surface Temperature in Polymer Gears and Its Relationship to Gear Wear. *J. Tribol.* **1993**, *115*, 119–124. [CrossRef]
19. Mao, K.; Li, W.; Hooke, C.J.; Walton, D. Polymer gear surface thermal wear and its performance prediction. *Tribol. Int.* **2010**, *43*, 433–439. [CrossRef]
20. Matkovič, S.; Kalin, M. Effects of slide-to-roll ratio and temperature on the tribological behaviour in polymer-steel contacts and a comparison with the performance of real-scale gears. *Wear* **2021**, *477*, 203789. [CrossRef]
21. Pogačnik, A.; Kalin, M. Parameters influencing the running-in and long-term tribological behaviour of polyamide (PA) against polyacetal (POM) and steel. *Wear* **2012**, *290–291*, 140–148. [CrossRef]
22. Hameed, Z.; Hong, Y.S.; Cho, Y.M.; Ahn, S.H.; Song, C.K. Condition monitoring and fault detection of wind turbines and related algorithms: A review. *Renew. Sustain. Energy Rev.* **2009**, *13*, 1–39. [CrossRef]
23. Ziaran, S.; Darula, R. Determination of the State of Wear of High Contact Ratio Gear Sets by Means of Spectrum and Cepstrum Analysis. *J. Vib. Acoust.* **2013**, *135*. [CrossRef]
24. Lebold, M.; McClintic, K.; Campbell, R.; Byington, C.; Maynard, K. Review of Vibration Analysis Methods for Gearbox Diagnostics and Prognostics. In Proceedings of the 54th Meeting of the Society for Machinery Failure Prevention Technology, Virginia Beach, VA, USA, 1–4 May 2000.
25. Večeř, P.; Kreidl, M.; Šmíd, R. Condition Indicators for Gearbox Condition Monitoring Systems. *Acta Polytech.* **2005**, *45*, 35–43. [CrossRef] [PubMed]
26. Amarnath, M.; Praveen Krishna, I.R.; Krishnamurthy, R. Experimental Investigations to Study the Effectiveness of Cepstral Features to Detect Surface Fatigue Wear Development in a FZG Spur Geared System Subjected to Accelerated Tests. *Arch. Acoust.* **2023**, *46*, 479–489. [CrossRef]
27. Evans, S.M.; Keogh, P.S. Efficiency and running temperature of a polymer–steel spur gear pair from slip/roll ratio fundamentals. *Tribol. Int.* **2016**, *97*, 379–389. [CrossRef]
28. Hu, C.; Smith, W.A.; Randall, R.B.; Peng, Z. Development of a gear vibration indicator and its application in gear wear monitoring. *Mech. Syst. Signal Process.* **2016**, *76–77*, 319–336. [CrossRef]
29. Mao, K.; Li, W.; Hooke, C.J.; Walton, D. Friction and wear behaviour of acetal and nylon gears. *Wear* **2009**, *267*, 639–645. [CrossRef]
30. Shannon, C.E. Communication in the Presence of Noise. *Proc. IRE* **1949**, *37*, 10–21. [CrossRef]